Proceedings of ASME Turbo Expo 2003
Power for Land, Sea, and Air
June 16–19, 2003, Atlanta, Georgia, USA

GT-2003-38140

FILM COOLING ANALYSIS USING DES TURBULENCE MODEL

Subrata Roy and Sagar Kapadia
Computational Plasma Dynamics Laboratory
Kettering University, Flint, MI 48504

James D. Heidmann
NASA Glenn Research Center
Cleveland, OH 44135

ABSTRACT

The complex dynamic nature of the spanwise vortices in film cooling of turbine blades makes it necessary to accurately model the flow field temporally and spatially using detailed simulation techniques like direct numerical simulation or large eddy simulation of turbulence. Although, the later requires less computational effort and thus can simulate flows at higher Reynolds number than direct simulation, both these methods remain very expensive. As a viable alternative, this paper presents a Spalart-Allamaras based detached eddy simulation (DES) that is applied to a film cooled flat plate for the first time. The numerical model uses an unstructured grid system to resolve the dynamic flow structures on both sides of the plate as well as inside the hole itself. Detailed computation of a single row of 35 degree round holes on a flat plate has been obtained for blowing ratio of 1.0, and a density ratio of 2.0. The DES solution is also benchmarked with Reynolds averaged Navier-Stokes formulation for the same blade-hole configuration. The comparison shows that the DES simulation, which makes no assumption of isotropy downstream of the hole, greatly enhances the realistic description of the dynamic mixing processes.

INTRODUCTION

In a variety of industrial applications the interaction of cool air jets with hot crossflow becomes important. Examples include vertical takeoff and landing (V/STOL) engineering and film cooling of gas turbine blades. Systematic investigation of such flowfield started in late 50s. Jordison [1], Fearn and Weston [2], Moussa, et al. [3], Andreopoulos and Rodi [4] studied isothermal jets into crossflow. For thermal flows, the resulting temperature downstream of the jet, the trajectory and physical path of the jet are critical design parameters. Specifically, the blades/vanes in propulsion gas turbine engines require film cooling to protect the airfoils from thermal stresses caused by exposure to hot combustion gases. The problem becomes aggravated by the growing trend to use higher turbine inlet temperature for better engine performance. Figure 1 shows the schematic of a single round jet injected in the crossflow at an angle. This geometry is very appropriate for the turbine engine community and has been extensively studied for cooling performance for a wide range of blowing ratio (i.e., momentum ratio of injected air to crossflow). These results show details of the vortex interaction region, and mixing and mean centerline species concentration decay in the near and far field.

Goldstein [5] summarized early studies in the area of film cooling. These studies were based on slot flows, and film cooling effectiveness values were found to correlate well with the parameter x/Mb, where x is the downstream distance, M is the blowing ratio, and b is the slot width. This parameter has also been used for discrete hole cooling, with b defined as the effective slot width for the row of holes. However, the physics of discrete hole cooling is quite different from that of a slot. A row of discrete holes typically has a much lower span averaged downstream film effectiveness distribution for the same x/Mb due to the formation of vortices which allow hot gas to penetrate to the wall. These vortices are of the scale of the hole size, so if a numerical simulation has a spanwise grid spacing greater than the film hole spanwise pitch, as is typical for turbine blade aerodynamic design, their effect is lost. In essence, any such calculation is two-dimensional on the scale of the film holes.

Numerical investigations of jets based on integral methods were done by Vizel and Mostinskii [6], Chen [7] and Adler and Baron [8] initially. These models were essentially idealized models. A number of numerical models have also been proposed that approximated the three-dimensional vortex sheet by a two-dimensional one to predict details of the flowfield [7]. However, the mixing of a jet in a cross-stream is a fully three-dimensional phenomenon (Moussa et al. [3], Fric and Roshko [9], Smith and Mungal [10]), and thus such idealized treatments lack accuracy. Numerical solutions of the full Navier-Stokes equations have also been used to obtain detailed solutions in

various studies. Early attempts by Chien and Schetz [11] used closure models based on constant turbulent viscosity. Amer et al. [12] pointed out that the flow predictions are greatly affected by the selection of the turbulence model. Later studies were based on the k-ε model of turbulence or its variants. These results indicate that the Reynolds averaged Navier-Stokes (RaNS) model gives predictions of engineering accuracy. Such predictions depend on M and the distance downstream from the injection holes. Rai [13] used non-isotropic models, based on algebraic expressions for the Reynolds stresses. Roy [14] documented the cooling performance of twelve different arrangements of holes with a combination of blowing ratio M, distance between the holes L and jet angle α using a upwind biased finite volume code and standard k-ε turbulence closure model. Numerical solutions for these flow arrangements document strong to moderate secondary vortex structures spanning normal to the direction of the jet. This fully three-dimensional flow field strongly influences the cooling performance of the hole-blade system. Computational results predict an optimum hole spacing and low issuing angle for maximum cooling efficiency.

Several computational studies have computed turbine blade geometries with accurate resolution of the film holes, and in some cases, of the hole pipes and plena as well. Garg and Gaugler [15] showed the importance of film hole exit profiles. Garg and Rigby [16] resolved the plenum and hole pipes for a three-row showerhead film cooling arrangement with Wilcox's k-ω turbulence model, and Heidmann et al. [17] used RaNS to compute the heat transfer for a realistic turbine vane with 12 rows of film cooling holes with shaped holes and plena resolved. Garg [18] presented results of a full rotating blade with 172 film holes, resolving the film hole exits, but not the hole pipes and plena. These studies provide good details of the flow. However, the anisotropic dynamic nature of the spanwise vortices that affect the film cooling process are more complex than that can be captured by the mixing models used in aforementioned papers.

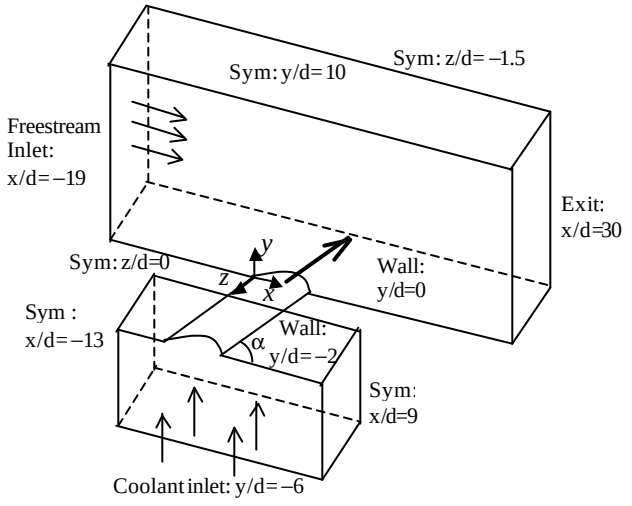

Figure 1. Schematic of the film cooling flow. Actual geometry definition and boundary conditions are based on Sinha et al. [19], Leylek and Zerkle [20].

In the near field of the film cooling jet, the dynamic large scale structures control the mixing process (Ho and Huerre [21]). This three-dimensional mixing determines the normal and transverse penetration of the jet. The accurate prediction of the jet penetration and reattachment location greatly influences the accuracy of the numerical prediction of the heat transfer process or the film cooling effectiveness on the adiabatic blade surface. The complex dynamic nature of the spanwise vortices makes it necessary to accurately model the flow field temporally and spatially using direct numerical simulation (DNS) or large eddy simulation (LES) of turbulence. Although, LES requires less computational effort or can simulate flows at higher Reynolds number than DNS, one major challenge for performing LES in film cooling is the range of length scales that must be resolved in the computation (Lesieur et al. [22]). Several subgrid models exist in the literature. However, based on the scales, LES remains very expensive.

As a viable alternative, this paper presents the first detached eddy simulation (DES) based modeling of film cooling flow for the three-dimensional geometry shown in Figure 1. DES is a hybrid turbulence model that works by applying a variable length scale that varies as a function of the distance to the nearest wall in the attached boundary layer and conforms with sub-grid scale in the rest of the flow including separated regions and near wake (Strelets, [23]). The literature indicates that the mixing processes downstream of the hole are highly anisotropic, as the turbulent diffusion is much stronger in the transverse direction (normal to the jet trajectory) than in the streamwise direction. This causes underprediction of jet spreading by the isotropic turbulence models like k-ω. The opportunity to utilize the DES simulations, which makes no such assumption of isotropy downstream of the hole, should greatly enhance the modeling efforts by providing a more realistic description of the mixing processes on which the model will be based. The paper also documents solution comparison of DES and RaNS models for blade-hole configuration.

NOMENCLATURE

A, B, C	Viscous terms
b	Slot width
C_{des}	Turbulence constant for S-A based DES model
d	Hole diameter
d_w	Distance to the nearest wall
$\vec{f}$	flux vector
F, G, H	flux vector components
L	Distance between hole centers
M	Blowing ratio
p	Pressure
q	Primary variable vector
Re	Reynolds Number
$\tilde{S}$	Production term
S	Value of vorticity
T	Static temperature

T_{fs} Hot free stream temperature

T_j Cool jet temperature

u_{fs} Free stream velocity

u X-component of the velocity

v Y-component of the velocity

w Z-component of the velocity

V Fluid element volume

Δx_i Mesh size in respective cartesian directions

y^+ inner variable

Greek

α Jet issuing angle

ε Turbulenct dissipation rate

δ Fluid element surface area

h Film cooling effectiveness, $\left(T_{fs} - T\right) \Big/ \left(T_{fs} - T_j\right)$

n Molecular viscosity

n_T Turbulence kinematic viscosity

$\tilde{n}$ Working variable

n^* Reference turbulent kinematic viscosity

r Density

θ Implicitness

TURBULENCE MODEL

The complex dynamic nature of the film cooling flow makes it necessary to model the vortices using temporally and spatially accurate calculation of the flow field to capture the dominant turbulence length scales. Various turbulence models are available in the literature (Tannehill et al. [24], Pope [25], Spalart [26]). The two competing factors important for any turbulence model are accuracy and efficiency (i.e. computational cost). An optimal combination of both these factors is hard to achieve and thus, the primary purpose of the numerical simulation is towards attaining such a goal. Numerical simulations in this study were performed using a finite volume based parallel, implicit, unstructured Euler/Navier-Stokes flow solver called Cobalt (Grismer et al. [27], Strang et al. [28], Kapadia et al. [29]). This code has proved very useful for high-speed, massively separated flows that are common in aerospace engineering.

RaNS, LES and DNS modeling

A brief discussion on available turbulence modeling techniques in terms of accuracy and computational cost is presented in this section.

Of all the available turbulence models, direct numerical simulation (DNS) is considered as the most accurate turbulent model. However, DNS explicitly accounts for all scales of motion in a turbulent flow, from the largest, imposed by the existence of boundaries or periodicities, to the smallest. Kim et al. [30] showed from that DNS of fully developed incompressible channel flow at a Reynolds number of about 6000 (based on channel height) requires grid with 2 and 4 million points. Wilcox [31] gave the following equation to estimate the number of grid points for channel flow.

$$N_{DNS} = (0.088 Re_h)^{9/4} \quad (1)$$

where Re_h is the Reynolds number based on the mean channel velocity and channel height. This imposes critical limitation on the applicability of DNS in high Reynolds number flows. By combining above equation with the available computational resources, one can conclude that it is impossible to apply DNS for complex 3-D turbulent flows using present day computers.

Large eddy simulation (LES) is also quite reliable to resolve unsteady turbulent flows (Ansari and Strang [32], Moin [33], Howard and Pourquie [34]). In LES large-scale structure of turbulent flow is computed directly and the smallest and nearly isotropic eddies are modeled as sub-grid scale eddies. Moin [33] has described numerical and physical issues involved in LES. Filter (space averaging) width is an important parameter in LES. For homogeneous turbulent flows, filter width remains constant in spatial direction. For inhomogeneous turbulent flows, (e.g. turbulent boundary layer, where size of the eddies near walls is smaller than the size of eddies present in the regions away from the wall) filter width becomes the function of the space. Ghosal [35] concluded that explicitly filtered equations gives satisfactory results with finite difference if filter width is larger than the cell size in the computational grid. Computational requirement for LES is approximately $(1/10)^{th}$ times of that of DNS. In spite of huge computational requirement, LES is being used nowadays for practical problems [34-37].

Reynolds average Navier-Stokes (RaNS) is considered as the most practical turbulence handling technique with the present day available computational resources. The Reynolds equations are derived by decomposing the dependent variables of Navier-Stokes conservation equations into time-mean and fluctuating components and then time averaging the entire equation. As equations are averaged in this technique, additional assumptions are required to close the system of equations, which forms the basis of RaNS turbulence modeling. This technique can be further classified and the most common classification is based on the number of supplementary partial differential equations that must be solved in order to supply the modeling parameters.

As described in the previous section, each turbulence model has its own benefits and drawbacks. But if one can combine the positive features of two or more models together to construct a single model, it would have more control in terms of both accuracy and computational cost. The same philosophy has been used in detached eddy simulation (DES). Proposed by Spalart et al. [38], DES is a hybrid model which combines RaNS and LES length scales to work under a single turbulence framework. Two different DES models (Strelets [23], Squires et al. [39]) are currently available in the numerical code used in the present simulation:

(1) S-A (Spalart-Allmaras) based DES model,

(2) M-SST (Menter's shear stress transport) based DES model.

Spalart-Allmaras based DES model is used in the present study. S-A model and S-A based DES formulations are discussed in following two sections.

Spalart-Allmaras (S-A) model

Spalart-Allmaras (Spalart and Allmaras [40]) is a one equation RaNS model, which is used in the present simulation. The S-A model solves a single partial differential equation for a variable $\tilde{n}$, which is related to the turbulent viscosity. The model is developed by Spalart and Allmaras [40], in which a transport equation for the turbulent viscosity is assembled, using empiricism and arguments of dimensional analysis, Galilean invariance and selected dependence on molecular viscosity.

The Spalart-Allmaras turbulent kinematic viscosity is given by

$$n_T = \tilde{n} f_{v1} \tag{2}$$

Following transport equation is used to calculate working variable $\tilde{n}$.

$$\frac{D\tilde{n}}{Dt} = c_{b1}[1 - f_{t2}]\tilde{S}\tilde{n} - \left[c_{w1} f_w - \frac{c_{b1}}{k^2} f_{t2}\right]\left[\frac{\tilde{n}}{d_w}\right]^2 \tag{3}$$
$$+ \frac{1}{s}\left[\nabla.((n+\tilde{n})\nabla\tilde{n}) + c_{b2}(\nabla\tilde{n})^2\right] + f_{t1}\Delta U^2$$

Eddy viscosity can be found out by using (2) and (3). The S-A model includes a wall destruction term to reduce the turbulent viscosity in the log layer and laminar sublayer. Trip terms are also provided in the model for smooth transition between laminar and turbulent flow. Constants and functions appear in (2) and (3) can be defined as following:

$$f_{v1} = \frac{c^3}{c^3 + c_{v1}^3}, \qquad c \equiv \frac{\tilde{n}}{n} \tag{4}$$

$\tilde{S}$ is a production term and can be express as,

$$\tilde{S} = f_{v3} S + \frac{\tilde{n}}{k^2 d_w^2} f_{v2}, \tag{5}$$

where S is the magnitude of the vorticity and

$$f_{v2} = \left[1 + \frac{c}{c_{v2}}\right]^{-3}, \tag{6}$$

$$f_{v3} = \frac{(1 + c\, f_{v1})(1 - f_{v2})}{c}, \tag{7}$$

From (5), (6) and (7), it can be seen that production term is different from that developed by Spalart and Allmaras (1992) due to the different formula of f_{v2} and new term f_{v3}. Now,

$$f_w = g\left[\frac{1 + c_{w3}^6}{g^6 + c_{w3}^6}\right]^{1/6}, \tag{8}$$

$$\text{where,} \quad g = r + c_{w2}(r^6 - r), \quad r \equiv \frac{\tilde{n}}{\tilde{S} k^2 d_w^2}. \tag{9}$$

Trip term f_{t1} is defined as,

$$f_{t1} = c_{t1} g_t \exp\left(-c_{t2}\frac{w_t^2}{\Delta U^2}\left[d_w^2 + g_t^2 d_t^2\right]\right) \tag{10}$$

where, d_t is the distance from the field point to the trip, ω_t is the wall vorticity at the trip and ΔU is the difference between the velocity at the field point and that at the trip.

$g_t = \min(0.1, \Delta U / w_t \Delta x)$, where Δx is the grid spacing along the wall at the trip. The function f_{t2} is defined as,

$$f_{t2} = c_{t3} \exp(-c_{t4} c^2). \tag{11}$$

Following constants are used in equation (2) to (11).

$c_{b1} = 0.1355,\ c_{b2} = 0.622,\ s = 2/3,\ k = 0.41,$

$c_{w1} = \frac{c_{b1}}{k^2} + \frac{1 + c_{b2}}{s},\ c_{w2} = 0.3,\ c_{w3} = 2,$

$c_{v1} = 7.1,\ c_{v2} = 5,\ c_{t1} = 1,\ c_{t2} = 2,\ c_{t3} = 1.1,\ c_{t4} = 2.$

Trip terms are not used in the simulation presented in this paper. Thus, transport equation (3) takes the following form for the case presented in this paper.

$$\frac{D\tilde{n}}{Dt} = c_{b1}\tilde{S}\tilde{n} - c_{w1} f_w \left[\frac{\tilde{n}}{d_w}\right]^2 + \frac{1}{s}\left[\nabla.((n+\tilde{n})\nabla\tilde{n}) + c_{b2}(\nabla\tilde{n})^2\right] \tag{12}$$

Detached eddy simulation

Present definition of DES, as described by Strelets [23], is not linked with any specific turbulence model. According to this definition, DES is a three-dimensional unsteady numerical solution using a single turbulence model, which functions as a subgrid-scale model in regions where grid density is fine enough for an LES, and as a RaNS model in regions where it is not. Spalart-Allmaras based DES model has been developed in such a way that the model works as S-A RaNS model near the wall surfaces and acts as a subgrid LES model away from the wall. RaNS is considered as an adequate and reliable technique to predict the flow in thin shear layers and LES has already proven to be powerful to predict the flow in large seaparted zones. Further, progress of unsteady RaNS (URaNS) in achieving accuracy is not much encouraging. Thus, DES combines LES and RaNS in such a way that RaNS technique can be used for the flow in thin shear layers and LES can be used for large separated zones for resolution of geometry-dependent and three-dimensional eddies.

In S-A based DES formulation, distance to the nearest wall, d_w is replaced by $\tilde{d}$, where $\tilde{d}$ is defined as,

$$\tilde{d} = \min(d_w, C_{DES}\Delta) \tag{13}$$

where, C_{DES} is a model constant and for S-A based DES model, C_{DES}=0.65 and Δ is the largest distance between the cell center under consideration and the cell center of the neighbors. The definition of the neighboring cells is given in the Algorithm section of the paper.

$$\Delta = \max(\Delta x, \Delta y, \Delta z). \tag{14}$$

Equation (13) and (14) keeps the DES model in RaNS S-A model inside the whole attached boundary layer as streamwise or spanwise or both grid spacing parallel to the wall are at least on the order of the boundary layer thickness and thus, in (13), $\tilde{d} = d_w$ and model works as a standard S-A turbulence model inside the boundary layer and the prediction of the boundary layer separation is also made by RaNS mode of DES. In the regions, far from the wall, where $d_w > C_{des}\Delta$, the length scale of the model becomes grid-dependent. The model performs as a subgrid-scale version of the S-A model for eddy viscosity. When production and destruction terms balance each other, this

model reduces to an algebraic mixing-length Smargorinski-like subgrid model. Recently, Forsythe et al. [41]and Kapadia et al. [26] have successfully implemented DES for external flow simulation over a fighter aircraft and an Ahmed reference car, respectively.

NUMERICAL METHOD

Algorithm

Godunov's [42] first-order accurate, exact Riemann method is the foundation of the present numerical scheme. Second-order spatial and temporal accuracies are achieved in the numerical simulations presented in the paper. Hansen and Forsythe [43] successfully compared the experimental results of flow over a circular cylinder for both subcritical and supercritical Reynolds number with the numerical results achieved by using present numerical scheme. This comparison shows the ability of the second order accurate discretization of the present unstructured solver to work in the LES mode of DES turbulence model. Size of the time-step is a function of CFL. Initial value of CFL is taken as 1000, which gradually increases to 1000000 after 500 timesteps and remains constant for further timesteps. Size of the timestep coreesponding to this CFL is 2.03 x 10^{-3}s. The cell-centered, finite-volume approach is used in the computational method. Implicit time stepping, viscous terms and turbulence models are added in the numerical model. Numerical model is compatible with all kinds of unstructured grids. Numerical code used for the simulation uses parallel algorithm. Thus, grid can be divided into groups of cells, or zones, for parallel processing. One feature of the numerical code merges different zones of the mesh to create a single zone grid.

Five fundamental tasks comprise the flow solution algorithm: Construction of initial conditions for the Riemann problem at any given face, solution of this Riemann problem, construction of viscous fluxes at any given face, time integration and boundary conditions. The first step, constructing the initial conditions for the Riemann problem, is critical to the algorithm, for it includes any limiting or dissipation and it largely determines the spatial accuracy and truncation error of the scheme.

The baseline RaNS calculations were performed using the NASA Glenn-HT code. These results were previously described in Heidmann and Hunter [44]. Briefly, the code solves the full compressible Reynolds-averaged Navier-Stokes equations. It employs the finite volume method with central differencing. The k-w turbulence model is used without wall functions, as the computational grid is sufficiently fine to yield y+ values of less than 1.0 at the first cell from the wall.

Numerical code used in the present simulation can be run for both first and second order spatial accuracy. For the first order spatial accuracy, constant data distribution is assumed in each cell. For the second order spatial accuracy, data distribution is assumed to be linear in each cell. Equation used to find out the left initial state of face J for Riemann problem with second order spatial accuracy is as following:

$$q_i^J = q_i + \vec{r}^J . \vec{\nabla} q \tag{15}$$

'*J*' and '*i*' denotes the face and cell respectively as described in the previous section. q_i^J is the estimated value at the centroid of face J due to cell *i*, $\vec{\nabla} q_i$ is the gradient vector and $\vec{r}_i^J$ is a vector from the centroid of the cell i and pointing towards the centroid of face *J*. The gradient vector for cell i is found by a least-squares solution to (15). Right initial state for face *J* can be found in the similar way.

Final equation in the matrix form after considering the nearest-neighbor cells is as following:

$$A\vec{\nabla}^c q_i = \{q_m - q_i\} \tag{16}$$

$\vec{\nabla}^c q_i$ is a central difference gradient and A is an over-determined matrix due to more number of nearest-neighbor cells (equations) than unknowns. Eq. (16) is solved by QR factorization. Following equation shows the temporal integration used in the numerical scheme.

$$q\left\{V\frac{dq}{dt} + \vec{\nabla}.\vec{f}\right\}_i^{n+1} + (1-q)\left\{V\frac{dq}{dt} + \vec{\nabla}.\vec{f}\right\}_i^{n} = 0 \tag{17}$$

where θ is the implicitness, $\vec{f}$ is a flux vector, n and (n+1) shows successive time-steps. Time integration scheme can be fully explicit for θ=0 and it can be fully implicit for θ=1.

Temporal derivatives in the discrete form for n^{th} and $(n+1)^{th}$ time-steps are as follows:

$$\left(\frac{\partial q}{\partial t}\right)^{n+1} = \frac{a_{1,1}(q^{n+1} - q^n) + a_{1,2}(q^n - q^{n-1})}{\Delta t} \tag{18}$$

$$\left(\frac{\partial q}{\partial t}\right)^{n} = \frac{a_{2,1}(q^{n+1} - q^n) + a_{2,2}(q^n - q^{n-1})}{\Delta t} \tag{19}$$

For the first order temporal accuracy, $\alpha_{1,1} = \alpha_{2,1} = 1$ and $\alpha_{1,2} = \alpha_{2,2} = 0$. For the second order accuracy, $\alpha_{1,1} = 3/2$, $\alpha_{1,2} = (-1/2)$, $\alpha_{2,1} = \alpha_{2,2} = 1/2$. For this problem, a second-order accurate time integration scheme is used. Finally, the semi-discrete form of the governing equation is given by,

$$V_i \frac{dq_i}{dt} + \sum_{M=1}^{N_i}\left(F^M \hat{i} + G^M \hat{j} + H^M \hat{k}\right)\hat{n}^M d^M = \sum_{M=1}^{N_i}\left(A^M \hat{i} + B^M \hat{j} + C^M \hat{k}\right)\hat{n}^M d^M \tag{20}$$

where the subscript *i* and superscript M denote quantities for the i^{th} cell and the M^{th} face of cell *i*, respectively, and N_i is the number of faces bounding cell *i*.

Grid information and computational approach

It is easy to appreciate the geometric complexity of realistic turbine blades as analyzed by Garg and Rigby [16]. In this paper, a simplified model is needed to verify the capability of DES in capturing the dynamic details of the spanwise mixing process. Many published studies have discussed the physics and presented data for discrete hole film cooling in simplified geometries. The most basic geometry consists of a row of round holes in a flat plate. There is a relatively large body of experimental data for 35 deg.-pitch round holes with a spacing of 3d (Foster and Lampard [45], Pietrzyk et al. [46], Pietrzyk et al. [47], Sinha, et al. [19], Heidmann and Hunter [43]). This

geometry allows for a study of jet lift-off behavior at various blowing ratios and is perhaps the most realistic simplified geometry for turbine film cooling. In addition, the computational study of Leylek and Zerkle [20] and Heidmann and Hunter [43] and the experimental data of Sinha et al. [19] use this geometry and give excellent description of the vortical flows associated with this geometry. The present study therefore uses this geometry for the film cooling detached eddy simulation.

A multi-block computational grid was initially developed using the GridPro multiples grid generator with 15 blocks and approximately 1,300,000 computational cells. Gridgn14.03 is used to convert this grid into Cobalt compatible unstructured grid. The final grid used in the solution contains single block and 899584 cells. Viscous clustering was employed at all solid walls with a y^+ value less than 1.0 at all locations. Stretching ratios less than 1.2 were used normal to the viscous walls. Convergence was considered achieved when both of the following criteria had been met: (a) reduction in all residuals of four orders of magnitude, and (b) no observable change in surface temperature prediction for an additional 30 iterations. It was found that the solution indeed required at least the resolution of this finer grid, since the calculation on the coarser grid underpredicted jet reattachment and film effectiveness. Because of computational limitations, the grid was not refined further.

Present case is run on the cluster of 256 parallel processors on Blue Horizon supercomputer at SDSC. The aggregate CPU time requirement for the entire DES solution is 11.02seconds/iteration and that for one cell is 12.25 micro seconds/iteration. The aggregate CPU time includes flow solution time, problem set-up time and restart file creation time. The presented case has been run for 6000 time-steps and corresponding total time of the solution is 11.7 seconds. Total CPU requirement for this solution is 1200 hrs.

RESULTS AND DISCUSSION

Figure 1 describes schematic control volume of hot air passing over a flat surface (e.g., a turbine blade). This surface of study has a row of injection holes through which the cool air is issued at an angle α=35°. The cool jet at temperature T_j =300K is injected into the hot freestream of T_{fs} =600K. The injection ducts are circular pipes with diameter equal to d=2.54mm. The injection hole formed by the intersection of the injection pipe with the wind tunnel is an ellipse with the minor and the major axes d and D=d/(sin α), respectively. The distance between the hole centers is L=3d. The selected mean flow velocities, static pressures and temperatures (i.e., densities) in the injection pipe and the wind tunnel gives a blowing ratio M=1. The inlet section is located at x=-19d and the exit at x=30d. The other dimensions and boundary conditions are shown in Figure 1. The flat (blade) surface is considered adiabatic.

Symmetry boundary conditions were employed in the spanwise direction, on all sides of the plenum, and at the y/d=10 plane. The use of the symmetry boundary condition at the hole and in the spanwise direction can be considered as a limitation of the simulation presented in this paper as it prevents the possibility of capturing the unsteady asymmetric vortical flow patterns. The large scale structures convecting downstream may induce these three-dimensional instability waves. Fixed mass flow rate and stagnation temperature inlet boundary conditions to the plenum and freestream were used to ensure proper density and blowing ratios. The inlet flows were normal to the inlet planes. Adiabatic no-slip conditions were applied at all solid walls, including the inner surface of the film hole and the plenum. A turbulence intensity of 0.5% and a turbulence length scale of 3% of the inlet height were used. The Reynolds number based on hole diameter and inlet conditions was 16100. An exit boundary condition with fixed static pressure was employed at x/d=30. A maximum Mach number not exceeding 0.3 was achieved in the flow field while maintaining the desired Reynolds number by scaling the experimental geometry down by a factor of 5. This resulted in a hole diameter of 2.54 mm, and was done to allow more rapid convergence of the solution using the density-based formulation of the computer code while minimizing compressibility effects.

In Figure 2, the velocity vectors colored by speed inside the injection pipe describes a stratification of kinetic energy inside the tube. After 2.8s, the instantaneous DES solution shows that most of the fluid is impinging at a high velocity (about 85m/s) on the left half of the tube. In the right half, the entrained fluid is creating a small recirculation (not explicit in the figure). Especially at the exit plane of the tube the flow is highly nonuniform. This is in agreement with the qualitative results of Heidmann and Hunter [43]. However, their RaNS solution is plotted as span-averaged data and therefore no direct comparison is done here with the present unsteady DES solution. Clearly, for this moderate blow ratio M=1 and a combination of flow profiles at the wind tunnel and cold jet inlet, the effect of the vorticity in the pipe is not negligible. This is due to the fact that at this range of velocities existing in the pipe, the boundary layers are not thin everywhere in the pipe. It is well known that coarse grids cannot resolve the effect of the downstream vortices.

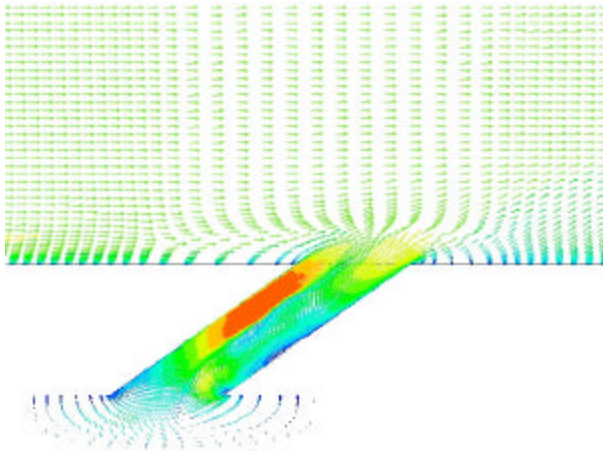

Figure 2. Instantaneous DES solution after 2.8s shows velocity vectors colored by fluid speed at the symmetry plane.

Heidmann and Hunter [43] pointed out that a more realistic description of the coolant boundary layer profile is needed in conjunction with downstream entrainment models to resolve the effect of the downstream vortices. However, a more realistic description of the coolant boundary layer profile at the hole exit - in the absence of a downstream mixing model - may actually worsen film effectiveness predictions compared to the current model due to a lower minimum jet temperature and lack of entrainment. DES presents that opportunity of realistic boundary layer description.

Corresponding flow field velocity vector distribution in the spanwise direction is shown in figure 3 at x= 5d. Both sides of the line of symmetry is plotted to depict the dominant bound vortical structure at this location. At 2.8s, the effect of the wind tunnel vorticity is significant. This is more pronounced in the *u*- and *v*-velocity profiles. The assumption of uniform velocity profile in the wind tunnel leads to higher *v*-values in the near-wall jet flow region. In this case, the maximum in the *u*-velocities is located below the maximum in the case of developed inlet profile in the wind tunnel. The tendency is that as the boundary layer in the wind tunnel becomes thicker, the velocity maxima appear at higher distances from the wall and the near-wall flow changes dramatically. At very thick boundary layers, the flow close to the wall behaves as a typical boundary layer, while for very thin incoming boundary layers a wall-jet flow exists downstream the jet exit.

For better understanding of the simulations, the multiple-jet flowfield can be divided into three areas: (i) The central jet, (ii) the near jet and (iii) the outside region. The jets coming out of the pipes appear to the incoming tunnel flow as "solid". A sharp velocity and temperature gradient is formed upstream of the jet while a "wake" region develops downstream of the jet. In the latter a pair of bound vortices per jet is formed, which bends the jet, producing the well-known kidney shape both in speed and temperature line contours. The stronger the vortices, the more distorted the jet cooling effect becomes.

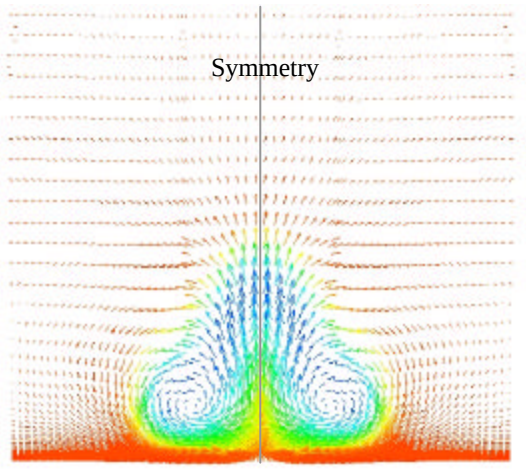

Figure 3. Velocity vectors at x/d = 5 after 2.8s shows the well-known kidney shape flow structures.

The speed contours on the vertical z = -0.1d plane after 2.8s demonstrates the mixing of boundary layer into the mainstream hot gas flow in figure 4. The red color in the vertical plane indicates a range of 78-85 m/s, which is dominant in the hot mainstream and in the cool jet pipe region. The spanwise vortical structures that are responsible for this mixing are dynamic and will be described later. The flat plate with hole with normalized temperature distribution T/T_{fs} ranging from 0.85 (blue) to 0.97 (green) is also shown in this figure. Responding to the near wall turbulent boundary layer, the cooling of the blade starts at a distance downstream of the jet exit, figure 4.

Figure 5 describes the temperature distribution on the same vertical plane where the speed contours were plotted in figure 4. After 2.8s solution time, the cool jet diffusion into the hot crossflow plots the wavy structure of the cold fluid boundary as it turbulently mixes with the hot combustion gas. Although the wave patterns are similar, a close observation shows there is a phase lag between the growth of fluid boundary layer and the thermal boundary layer. The red in figure 5 represents $T/T_{fs}=1$, yellow is 0.9, green is 0.7 while the blue is 0.5.

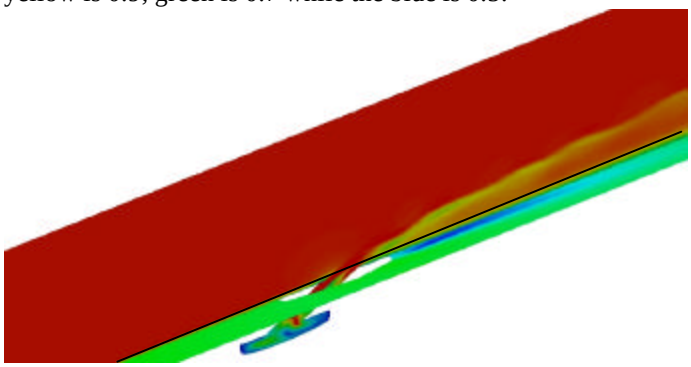

Figure 4. Instantaneous speed contours at z=-0.1d and temperature contours on the plate (y=0) after 2.8s.

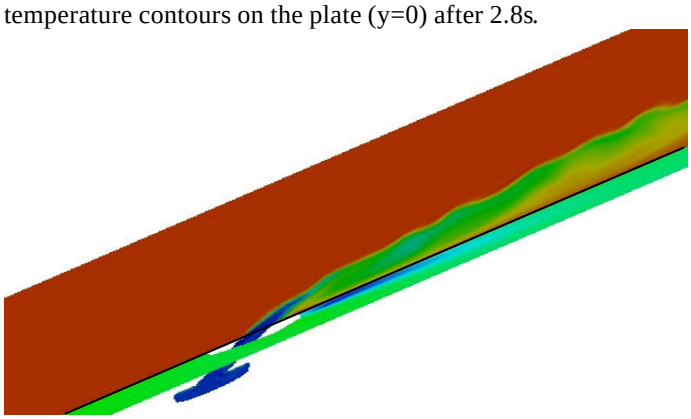

Figure 5. Instantaneous temperature contours on z=-0.1d and y=0 after 2.8s show growth of thermal boundary layer.

Since the DES solution is inherently unsteady and involves fluctuating components, it is important to run the simulation to a quasi-stationary state where the solution does not evolve beyond a preset criteria. For the present problem, the solution reaches such a state beyond 11.7s. Figure 6 documents the time history of the DES solution mass flow rate per unit area crossing the exit plane at x =30d. The inset clearly shows the unsteady nature of the flow. In order to compare DES results

with a RaNS solution, it is crucial that one determines the time-averaged data for DES. A direct comparison between the steady RaNS solution with the time-averaged and instantaneous DES solution is shown in figures 7-9.

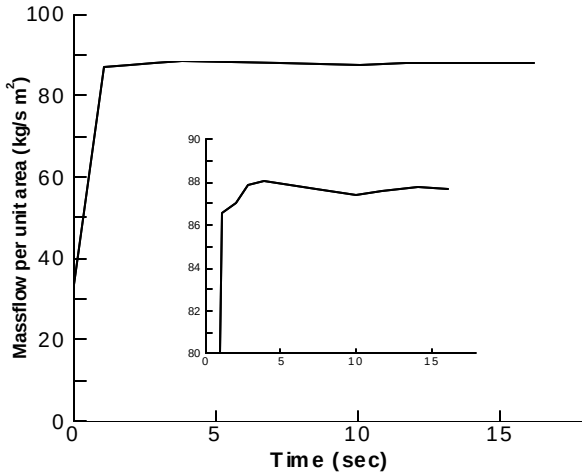

Figure 6. Time history of the mass flow rate at the exit.

Figure 7a-c documents the development of the quasi-stationary thermal boundary layer after 11.7s and its time averaged distribution. In all three plots, the inlet temperature of free stream hot gas normalizes the temperature contours. As the cool jet penetrates the hot gas, three-dimensional mixing occurs at the edge of the thermal boundary layer. The RaNS solution in figure 7a shows a thin boundary layer as compared to the time averaged DES result in figure 7c.

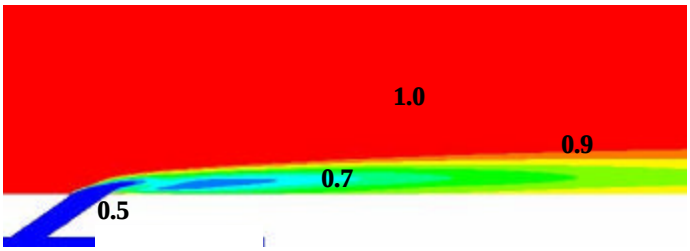

(a) RaNS solution at steady state

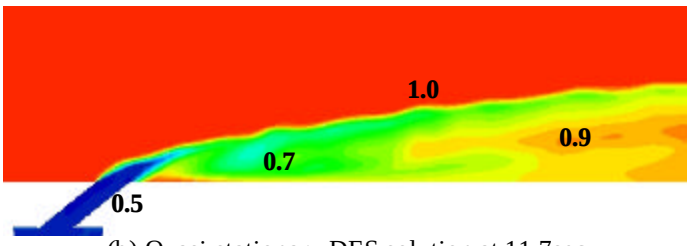

(b) Quasi-stationary DES solution at 11.7sec

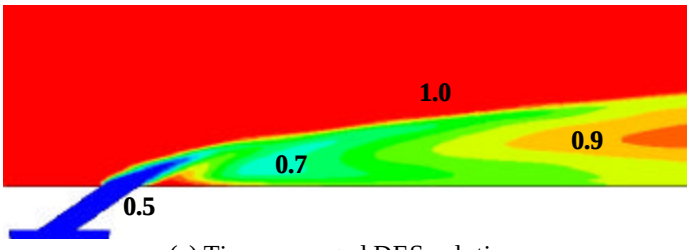

(c) Time-averaged DES solution

Figure 7. Comparison of normalized temperature contours for RaNS and DES solutions.

As expected, both the instantaneous (figure 7b) and time-averaged (figure 7c) DES solution shows deeper penetration due to three-dimensional mixing of the jet. The dynamic nature of the mixing process is evident from the wavy fingerlike structures of the instantaneous DES solution temperature contours in figure 7b. At z=–0.1d the distribution of temperature shows that just downstream of the jet exit remains hot (T/T_{fs}=1.0), beyond which the bound vortices pulls the coolant down to the flat surface. The normalized temperature for the rest of the boundary layer ranges from 0.7 to 0.9.

Blade temperature prediction is the primary interest for film cooling analysis. Figure 8a-b plots the steady state RaNS solution and the DES solution time-averaged at 11.7s. The time averaging of the DES solution began at 0.0001s. It is evident that the RaNS solution in figure 8a is far more diffused near the jet while the time-averaged DES solution in figure 8b is cooling further downstream. A detailed understanding of this comparison will be possible through the analysis of the effectiveness (see figure 10).

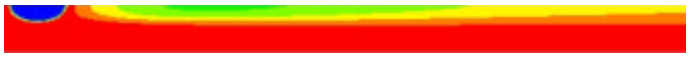

(a) Steady RaNS solution

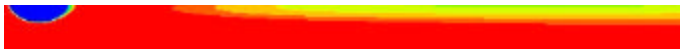

(b) Time-averaged DES solution

Figure 8. Comparison of temperature distribution on the flat plate (y/d=0).

Since film cooling is a strongly coupled fluid-thermal process, the effect of flow structures on fluid temperature distribution is plotted at x=5d in figure 9a-c. While figure 9a plots the RaNS solution at steady state, figures 9b and 9c show the quasi-stationary and time-averaged DES results on the same plane. The evolution of flow structure between 2.8s (figure 3) and 11.7s is noticeable (figure 9b). The RaNS solution in figure 9a is quite diffused as is evident from the temperature contours. In comparison, both the quasi-stationary solution 11.7s and the time-averaged data show prominent features of elongated kidney-shaped bound vortex (symmetric half) followed by similar temperature profiles. At the center of this vortex is the coolest region of T/T_{fs}=0.5 while outside the vortical structure the temperature is that of free stream hot gas. The turbulent diffusion is much stronger in transverse direction (normal to the jet trajectory) than in the streamwise direction. Likewise the temperature contour lines in high temperature region document anisotropic nature of the mixing process on this plane.

Finally in Figure 10, the film cooling effectiveness η calculated via time-averaged DES and RaNS solution is benchmarked with the experimental data [19]. The laterally averaged effectiveness distribution in the streamwise direction shows good matching of RaNS and DES solutions upto about x=2d. While the effectiveness computed from RaNS solution is comparable with the experimental data at x = 5d, in the downstream region of the flow the prediction bifurcates. As x ≥12d, the time-averaged DES prediction becomes more reasonable.

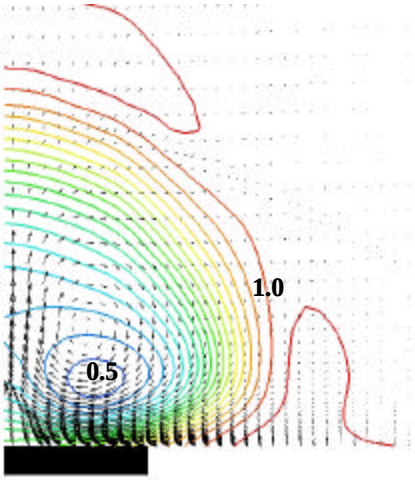

Figure 9a. Steady RaNS solution velocity vectors with superimposed temperature contour lines at x/d = 5.

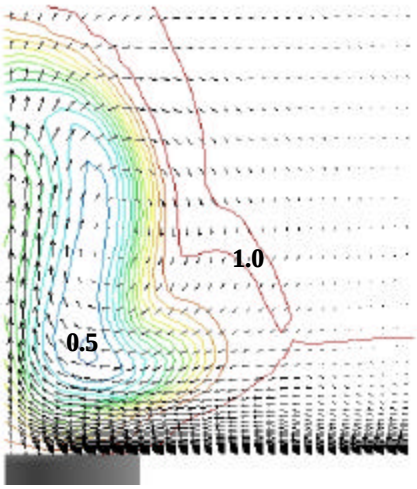

Figure 9b. Quasi-stationary DES solution velocity vectors with superimposed temperature contour lines at x/d = 5 after 11.7s.

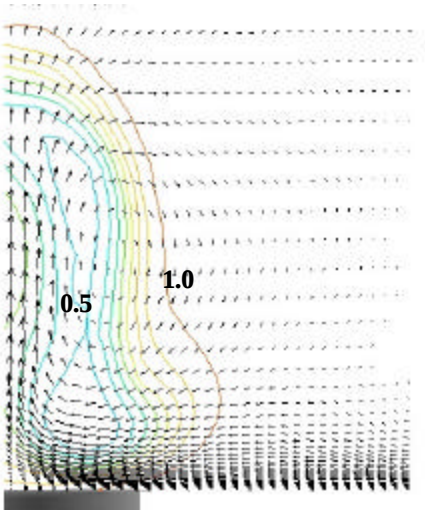

Figure 9c. Velocity vectors with superimposed temperature contour lines at x/d = 5 for time-averaged DES solution

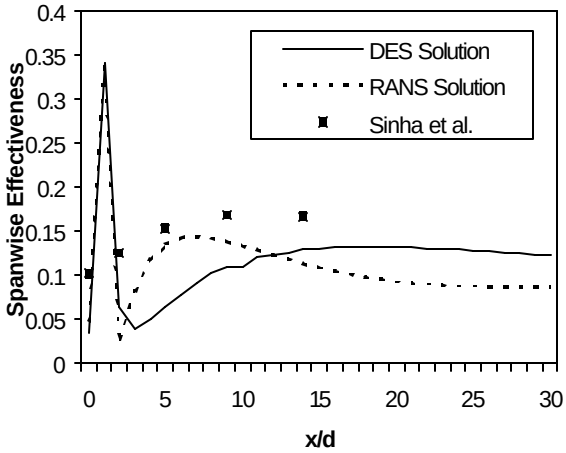

Figure 10. Comparison between experimental and numerical (DES and RaNS) values of spanwise-averaged effectiveness.

CONCLUSION

The first detached eddy simulation of film cooling has been presented for a widely published blade-pipe configuration. The blowing ratio was unity. Results indicate that the mixing processes downstream of the hole are highly anisotropic, as the turbulent diffusion is much stronger in the transverse direction. In comparison to the RaNS solution temperature distribution on the blade and near the vertical symmetry plane, DES should capture better description of the dynamic flow structures. However, the symmetry boundary condition used in this simulation might have inhibited the growth of three-dimensional asymmetric instability deterring further mixing. The following two improvements are key for future DES simulation in film cooling applications: (i) Grid independence study. (ii) Removal of symmetry boundary conditions. In order to truly understand these solution improvements, investigations will also be necessary for varying jet configurations.

ACKNOWLEDGMENTS

This research was supported in part by NASA Grant no. NAG3-2843 and NSF cooperative agreement ACI-9619020 through computing resources provided by the National Partnership for Advanced Computational Infrastructure at the San Diego Supercomputer Center.

REFERENCES

[1] Jordison, R., 1958, "Flow in a jet directed normal to the wind," *Aero. Res. Council, R & M.*, No. 3074.
[2] Fearn R., and Weston, R. P., 1974, "Vorticity associated with a jet in a cross flow," *AIAA Journal*, 12, pp. 1666-1671.
[3] Moussa, Z. M., Trischka, J. W., and Eskinazi, S., 1977, "The near field in the mixing of a round jet with a cross-stream," *J. Fluid Mech.*, 80, pp. 49-80.
[4] Andreopoulos, J., and Rodi, W., 1984, "Experimental investigation of jets in a crossflow, *J. Fluid. Mech.*, 138, pp. 93-127.
[5] Goldstein, R. J., 1971, "Film Cooling, Advances in Heat Transfer," Vol. 7, Academic press, New York, pp. 321-379.
[6] Vizel, Y. M., and Mostinskii, I. L., 1965, "Deflection of a jet injected into a stream," *Fluid Dynamics*, 8, pp. 127-139.

[7] Chen, C. L. H., 1942, "Aufrollung eines zylindrischen strahles durch querwind," Ph.D. Thesis, University of Gottingen.
[8] Adler, D., and Baron, A., 1979, "Prediction of a three-dimensional circular turbulent jet in a crossflow," *AIAA Journal*, 17, pp. 168-174.
[9] Fric, T. F., and Rosko, A., 1994, "Vortical structure in the wake of a transverse jet," *J. Fluid Mechanics*, 279, pp. 1-47.
[10] Smith, S. H., and Mungal, M. G., 1998, " Mixing, structure and scaling of the jet in crossflow," J. *Fluid Mech.,* 357, pp. 83-122.
[11] Chien J. C., and Schetz, J. A., 1975, " Numerical solution of the three dimensional Navier-Stokes equations with applications to channel flows and a buoyant jet in a cross flow," *ASME J. Appl. Mech.*, 42, pp. 575-579.
[12] Amer, B., Jubran, A., and Hamdan, M. A., 1992, "Comparison of different two-equation turbulence models for prediction of film cooling from two rows of holes," *Numerical Heat Transfer, Part A*, 21, pp. 143-162.
[13] Rai, M. M., 1987, "Navier-Stokes simulations of blade-vortex interaction using high-order accurate upwind schemes," *AIAA Paper 87-0543*.
[14] Roy, S., 2000, "Numerical Investigation of the Blade Cooling Effect by Multiple Jets Issuing at an angle," *J. Num. Heat Transfer*, 38, no. 7, pp. 701-718.
[15] Garg, V. K., and Gaugler, R. E., 1997, "Effect of Velocity and Temperature Distribution at the Hole Exit on Film Cooling of Turbine Blades," J. Turbomachinery, 119, pp. 343-351.
[16] Garg, V. K., and Rigby, D. L., 1999, "Heat Transfer on a Film-Cooled Blade - Effect of Hole Physics," Int. J. Heat and Fluid Flow, 20, pp.10-25.
[17] Heidmann, J. D., Rigby, D. L., and Ameri, A. A., 2000, "A Three-Dimensional Coupled Internal/External Simulation of a Film-Cooled Turbine Vane," J. Turbomachinery, 122, pp. 348-359.
[18] Garg, V. K., 2000, "Heat Transfer on a Film-Cooled Rotating Blade," Int. J. Heat and Fluid Flow, 21, pp. 134-145.
[19] Sinha, A. K., Bogard, D. G., and Crawford, M. E., 1991, "Film-Cooling Effectiveness Downstream of a Single Row of Holes With Variable Density Ratio," J. Turbomachinery, 113, pp. 442-449.
[20] Leylek, J. H., and Zerkle, R. D., 1994, "Discrete-Jet Film Cooling: A Comparison of Computational Results with Experiments," J. Turbomachinery, Vol. 111, pp. 358-368.
[21] Ho, C.M., and Huerre, P., 1984, "Perturbed Free Shear Layers," *Ann. Rev. Fluid Mech*., 16, pp. 365-424, 1984.
[22] Lesieur, M., Comte, P., Lamballais, E., Métais, O., and Silvestrini, G., 1997, "Large-eddy simulations of shear flows," J. *Eng. Math.* ,32, pp. 195-215.
[23] Strelets, M., 2001, "Detached Eddy Simulation of Massively Separated Flows," AIAA Paper 01-0879.
[24] Tannehill, J. C., Anderson, D. A., and Pletcher, R. H., 1997, "Computational Fluid Mechanics and Heat Transfer, Second Edition," Taylor & Francis, Philadelphia.
[25] Pope, S. B., 2000, "Turbulent Flows," Cambridge University Press, Cambridge, United Kingdom.
[26] Spalart, P. R., 2000, "Trends In Turbulence Treatment," AIAA Paper 00-2306.
[27] Grismer, M. J., Strang, W. Z., Tomaro, R. F., and Witzeman, F. C., 1998, "Cobalt: A parallel, implicit, unstructured Euler/Navier-Stokes solver," Advances in Engineering Software, 29, 3-6, 365-373.
[28] Strang, W. Z., Tomaro, R. F., and Grismer, M. J., 1999, "The Defining Methods of $Cobalt_{60}$: A Parallel, Implicit, Unstructured Euler/Navier-Stokes Flow Solver," AIAA Paper 99-16635.
[29] Kapadia, S., Roy, S., and Wurtzler, K., 2003, "Detached Eddy Simulation Over a Reference Ahmed Car Model," AIAA Paper 2003-0857.
[30] Kim, J., Moin, P., and Moser, R., 1987, "Turbulence Statistics in Fully Developed Channel Flow at Low Reynolds Number," J. Fluid Mech. 177, 133-166.
[31] Wilcox, D. C., 1993, "Turbulence Modeling for CFD," DCW Industries, La Canada, California.
[32] Ansari, A., and Strang, W. Z., 1996, "Large-eddy simulation of turbulent mixing layers," AIAA Paper 96-0684.
[33] Moin, P., 1998, "Numerical and Physical Issues in Large Eddy Simulation of Turbulent Flows," JSME International Journal, 41, 2.
[34] Howard, R. J. A., and Pourquie, M., 2002, "Large eddy simulation of an Ahmed reference model," J. Turbulence, 3, 012.
[35] Ghosal, S., 1996, "An analysis of numerical errors in Large Eddy Simulation of Turbulence," J. Comp. Phys., 125, pp. 187-206.
[36] Ahmed, S. R., Ramm, G., and Faltin, G., 1984, "Some Salient Features of the Time-Averaged Ground Vehicle Wake," SAE Paper 840 300.
[37] Akselvoll, K., and Moin, P., 1995, "Large Eddy Simulation of Turbulent Confined Coannular Jets and Turbulent Flow over a Backward Facing Step," Report TF-63, Department of Mechanical Engineering, Stanford University, Stanford, CA 94305.
[38] Spalart, P. R., Jou. W-H., Strelets, M., and Allmaras, S. R., 1997, "Comments on the Feasibility of LES for Wings, and on a Hybrid RaNS/LES Approach," Advances in DNS/LES, 1st AFOSR Int. Conf. on DNS/LES, Aug 4-8, Greyden Press, Columbus, Ohio.
[39] Squires, K. D., Forsythe, J. R., Morton, S. A., Strang, W. Z., Wurtzler, K. E., Tomaro, R. F., Grismer, M. J., and Spalart, P. R., 2002, "Progress on Detached-Eddy Simulation of Massively Separated Flows," AIAA Paper 02-1021.
[40] Spalart, P. R., and Allmaras, S. R., 1992, "A One-Equation Turbulence Model for Aerodynamic Flows," AIAA Paper 92-0439.
[41]Forsythe, J. R., Squires, K. D., Wurtzler, K. E., and Spalart, P. M., 2002, "Detached-Eddy Simulation of Fighter Aircraft at High Alpha," AIAA Paper 02-0591.
[42] Godunov, S. K., 1979, "A difference scheme for numerical computation of discontinuous solution of hydrodynamic equations," J. Computational Physics, 32, 101-136.
[43] Heidmann, J. D., and Hunter, S. D., 2001, "Coarse Grid Modeling of Turbine Film Cooling flows using Volumetric Source Terms," ASME Paper 2001-GT-0138.
[44] Hansen, R. P., and Forsythe, J. R., 2003, "Large and Detached Eddy Simulations of a Circular Cylinder using Unstructured Grids," AIAA Paper 2003-0775.
[45] Foster, N. W., and Lampard, D., 1980, "The Flow and Film Cooling Effectiveness Following Injection Through a Row of Holes," J. of Engineering for Power, 102, pp. 584-588.
[46] Pietrzyk, J. R., Bogard, D. G., and Crawford, M. E., 1989, "Hydrodynamic Measurements of Jets in a Crossflow for Gas Turbine Film Cooling Applications," J. Turbomachinery, Vol. 111, pp. 139-145.
[47] Pietrzyk, J. R., Bogard, D. G., and Crawford, M. E., 1990, "Effects of Density Ratio on the Hydrodynamics of Film Cooling," J. Turbomachinery, Vol. 112, pp. 437-443.

